RESEARCH PAPER

CrossMark

The effect of postweld heat treatment on hydrogen-assisted cracking of 8630/Alloy 625 overlay

Tao Dai[1] · John C. Lippold[1]

Abstract

The weld interface of Alloy 625 clad onto AISI 8630 steel requires postweld heat treatment (PWHT) to reduce the heat-affected zone (HAZ) hardness of the steel to meet industry standards. This PWHT results in carbon diffusion and pile up in the transition zone at the fusion boundary which potentially embrittles the 8630/625 interface. For the 8630/625 overlay, the PWHT needs to be carefully selected to reduce the potential for hydrogen-assisted cracking (HAC) and/or sulfide stress cracking (SSC). In this work, a wide range of PWHT conditions defined by the Hollomon-Jaffe parameter (HJP) was studied using the delayed hydrogen cracking test (DHCT). The effect of PWHT on HAC behavior was quantified using this test and the optimal HJP range for resistance to HAC was determined to be in the range from 18,500 to 19,500. Fracture surface analysis was conducted on failed samples to further evaluate the effect of PWHT and confirm the optimal HJP range. The HAC behavior of the 8630/625 overlay was compared with that of the F22/625 overlay reported previously.

1 Introduction

Alloy 625 weld overlay on both AISI 8630 and F22 (2.25Cr-1Mo) steel has been widely used in the oil and gas industry for corrosion protection [1]. In as-welded condition, the heat-affected zone (HAZ) in base metal contains high hardness martensite and it is susceptible to hydrogen-assisted cracking (HAC) and/or sulfide stress cracking (SSC) [2]. The National Association of Corrosion Engineers (NACE) standard MR0175 and the International Standards Organization (ISO) 15156 [3] require that the HAZ hardness should be less than 22HRC or 250 VHN. As a result, postweld heat treatment (PWHT) is applied to reduce the HAZ hardness, but this PWHT drives carbon from the steel base metal into the transition zone [4]. Carbon "pile up" occurs at the transition zone due to the difference in diffusivity and forms a narrow, high

hardness region which will potentially cause HAC and/or SSC [4]. Thus, it is desirable to find an optimal PWHT that softens the HAZ while preventing embrittlement of the transition zone. In order to identify an optimal PWHT range, the effect of PWHT on HAC behavior of AISI 8630/Alloy 625 (or 8630/625) dissimilar metal weld (DMW) needs to be investigated. The use of an HAC test, such as the delayed hydrogen cracking test (DHCT), can potentially be used to predict the SSC behavior of the 8630/625 DMW.

A previous paper reported the effect of PWHT on HAC behavior of F22/625 DMW [1]. The results presented here for the 8630/625 uses a similar approach and will serve to compare and contrast PWHT behavior with that of F22/625 DMW samples. The HAC test method for the F22/625 DMW samples was the DHCT [1, 5, 6]. The DHCT uses a constant load and better simulates the practical scenario of HAC relative to the dynamic slow strain rate tensile test [7–9] or the single-end notched bend test [10–13]. The DHCT is also a reliable HAC test system, because there are only a few parameters that need to be controlled: charging current density, hydrogen charging solution type and pH, temperature, the amount of hydrogen recombination poison, and sample load (stress) [1]. In this study, DHCT parameters were selected based on previous research and/or through trial and error [1, 6]. They were kept constant for all the F22/625 DMW samples in different PWHT conditions [1].

Recommended for publication by Commission X - Structural Performances of Welded Joints - Fracture Avoidance

✉ Tao Dai
daitao11@gmail.com

1   Welding Engineering Laboratory, Department of Materials Science and Engineering, The Ohio State University, Columbus, OH, USA

Previous researchers conducted extensive material characterization and HAC testing of the 8630/625 DMW in the as-welded and PWHTed conditions [2, 4, 6, 10, 11]. Their work built a good foundation for the work reported here, but none has studied the effect of a wide range PWHT conditions on HAC behavior. Fenske [10] and Dodge [11] studied the effect of PWHT on HAC using the three-point bend test, but they both studied only three PWHT conditions and did not identify an optimal PWHT range with relative maximum HAC resistance in their studied parameter range. Fracture morphology of the failed samples was also studied by previous researchers [4, 6, 10, 11]. They only selected several fracture morphologies of interest for description and discussion. None of these studies provided an overview of the fracture surface or quantitatively measured the area variation of different fracture morphologies. The features of each typical type of fracture morphology were not presented systematically and the effect of PWHT on the variation of fracture morphology was not reported.

There is not a unified mechanism which can explain all the HAC phenomena that occur in structural materials [14]. The proposed mechanisms include (1) hydride-induced embrittlement [15], (2) hydrogen-enhanced localized plasticity (HELP) [15], (3) adsorption-induced dislocation-emission (AIDE) [16, 17], and (4) hydrogen-enhanced decohesion (HEDE) [18–25]. Beachem's theory [26] describes the variation of HAC fracture morphology as a function of hydrogen content and the stress intensity factor, but it does not address microstructural effects on HAC. Also, his theory was developed for steels [27], but may not apply to nickel alloy/steel dissimilar welds where different fracture morphologies are observed that are not included in this theory [1].

In this study, the DHCT was used to evaluate 8630/625 DMW samples in order to provide a direct comparison of HAC behavior with F22/625 DMW. Fenske [10] and Dodge [11] respectively only studied three PWHT conditions in their work, but a much wider range of PWHT (11 PWHTs including the as-welded condition) was tested to determine the optimal PWHT conditions with maximum HAC resistance. Thorough and systematic fractographic analysis was conducted on failed DHCT samples to determine the effect of PWHT on HAC behavior. The overall objective of this work is to determine the optimal PWHT range with highest HAC resistance.

2 Experimental procedures

2.1 Material

The 8630 steel was in the form of a forged pipe with 11-in. (307 mm) diameter and nominal 2.04-in. (52 mm) wall thickness. The Alloy 625 (AWS ERNiCrMo-3) weld overlay was

Table 1 Welding parameters used for overlay of Alloy 625 on 8630 steel forging

Parameter	Value	Parameter	Value
Step increment	0.150 in or 3.81 mm	Interpass temperature	550 °F or 287.8 °C
Voltage	11.0 V	Travel speed	7.9 in/min or 200.66 mm/min
Peak current	240.0 A	Hot wire peak current	179.0 A
Background current	120.0 A	Hot wire background current	55.0 A
Hot wire voltage	3.3 V	Heat input	10.0 kJ/in or 0.394 kJ/mm
Wire feed speed	66.9–82.2 in./min or 170–208.8 cm/min	Deposition rate	2.0 lb./h or 0.907 kg/h
Preheat temperature	350 °F or 176.7 °C	Shielding gas flow rate (Argon)	30.0 cfh or 14.17 L/min

Fig. 1 **a** 8630/625 dissimilar metal weld coupon. **b** Coupon after EDM machining of DHCT samples

(a)

(b)

performed using the hot-wire gas tungsten arc welding (HW-GTAW) process with the parameters listed in Table 1. The thickness of the overlay is 1.74 in. (44.2 mm), larger than that used in practice (Fig. 1a), in order to allow the machining of DHCT samples for hydrogen cracking tests with the fusion boundary in the center of the gauge section. The compositions of the 8630 steel and Alloy 625 filler metal are listed in Table 2. The mechanical properties of base metal, filler metal, and the overall weld sample in the as-welded condition are listed in Table 3.

2.2 Sample preparation

Electro-discharge machining (EDM) was utilized to machine the samples from the weld coupon as shown in Fig. 1b with the sample geometry shown in Fig. 2. The sample gauge section was wide enough to include multiple weld bead layers. The 8630/625 sample geometry used here is identical to the F22/625 sample reported in a previous paper [1]. The sample corners in the gauge section were square and did not employ the rounded edge used by Bourgeois [6]. Both square and rounded edge samples were evaluated in this work and their performance was found to be similar.

2.3 Postweld heat treatment conditions

The two PWHT parameters are temperature (T) in Kelvin and time (t) in hours. They can be combined in Eq. 1 to calculate the Hollomon-Jaffe parameter (HJP), which is a quantitative measurement of the tempering response of a PWHT.

$$\text{HJP} = T*(20 + \log t) \qquad (\text{Eq.1})$$

Hollomon-Jaffe parameter (HJP) for steel tempering treatments [28]

Eleven PWHT conditions were selected to study the effect of a wide range of HJP on hydrogen cracking behavior of the 8630/625 DMW samples (Table 4). Obviously, not all of these PWHT conditions are applicable in practice, especially those at lower temperatures (< 600 °C) or excessively long times. They were selected in order to study the extremes of the HJP for research purposes. The PWHT condition 630 °C/3.53 h has the same HJP = 18,555 as that of PWHT condition 620 °C/6 h, in order to study the effect of different PWHT conditions with equivalent HJP on the hydrogen cracking behavior. For each PWHT condition, at least two samples were prepared for DHCT except 630 °C/3.5 h. The PWHTs were conducted in a horizontal tube furnace (Lindberg 59,544) fitted with titanium sponge and filled with argon to reduce oxidation of the samples. A type K thermocouple was used for temperature control, especially to measure the heating time to the target temperature. Approximately 10–20 min was required for the samples to reach the target temperature immediately and this time was not included in the HJP. The samples were quenched in room temperature water at the end the PWHT.

2.4 Delayed hydrogen cracking test

The delayed hydrogen cracking test was developed in Ohio State University and was used in this investigation to evaluate the hydrogen cracking behavior (Fig. 3a). During the

Table 2 Chemical composition of 8630 steel and filler metal Alloy 625

	C	Ni	Cr	Mn	Si	Mo	S	P	Al	Cu	Ti	Nb	V	Ta	Fe
8630	0.32	0.86	0.97	0.90	0.32	0.41	0.009	0.008	0.026	0.17	0.002	–	0.032	–	bal.
625	< 0.01	64.0	22.7	< 0.01	0.04	9.0	0.001	< 0.01	0.12	< 0.01	0.23	3.59	–	0.004	0.3

Table 3 Mechanical properties of 8630, Alloy 625, and dissimilar overlay

	Ultimate tensile strength	Actual yield strength	%EL	%RA	Note
BM 8630	116 ksi or 800 MPa	98.3 ksi or 677.7 MPa	23.0	69.1	Provided by Cameron
FM 625	114 ksi or 786 MPa	85.0 ksi or 586 MPa	–	–	Provided by Acute
8630/625 as-welded	102 ksi or 703.3 MPa	63.2 ksi 435.7 MPa	9.75	49.13	Tested at Ohio State Uni, failure in the BM

test, a constant load was applied, which is amplified with a 10:1 leverage as shown in Fig. 3c. The sample gauge section was polished with #600 sandpaper to remove the oxide layer and cleaned with ethanol to remove contaminants. The sample was covered with plastic dip coating and only 0.125-in. (3.175 mm) weld metal, fusion boundary, and 0.375-in. (9.525 mm) base metal in the gauge section was exposed. The sample was immersed in a hydrogen-charging solution as the cathode as shown in Fig. 3b and d. The hydrogen-charging solution is a sulfuric acid solution with pH = 1.74 ± 0.02 (10 mL H_2SO_4 added in 10 l distilled water or 0.01859 mol/L), in addition of 5 g $Na_2S_2O_3$ as the hydrogen recombination poison. The platinum wire wound around the sample is the anode. Positive hydrogen ions migrated to the cathode and obtained electrons to form hydrogen atoms or hydrogen gas. With the help of hydrogen recombination poison, the hydrogen atoms penetrated into the exposed sample. In this work, the constant load is 40 ksi (275.8 MPa).

All tests were conducted 24 h after preparing the hydrogen-charging solution. Testing was performed at the ambient temperature, nominally 22 ± 2 °C. The constant charging current is kept at 10 mA/cm². Other experimental details and discussion of the DHCT procedure can be found in [1].

2.5 Fractography and identifying crack initiation location

After failure in the DHCT, the sample was removed from the hydrogen-charging solution as soon as possible to reduce corrosion. It was immediately rinsed with water and ethanol, hot-air dried, and ultrasonically cleaned. SEM Quanta 200 and EDX analysis were used to characterize the morphology and chemical composition of the fracture surface. The fracture surface of the half sample with Alloy 625 was analyzed due to probably more corrosion on the base metal side. Multiple samples were evaluated in each PWHT condition.
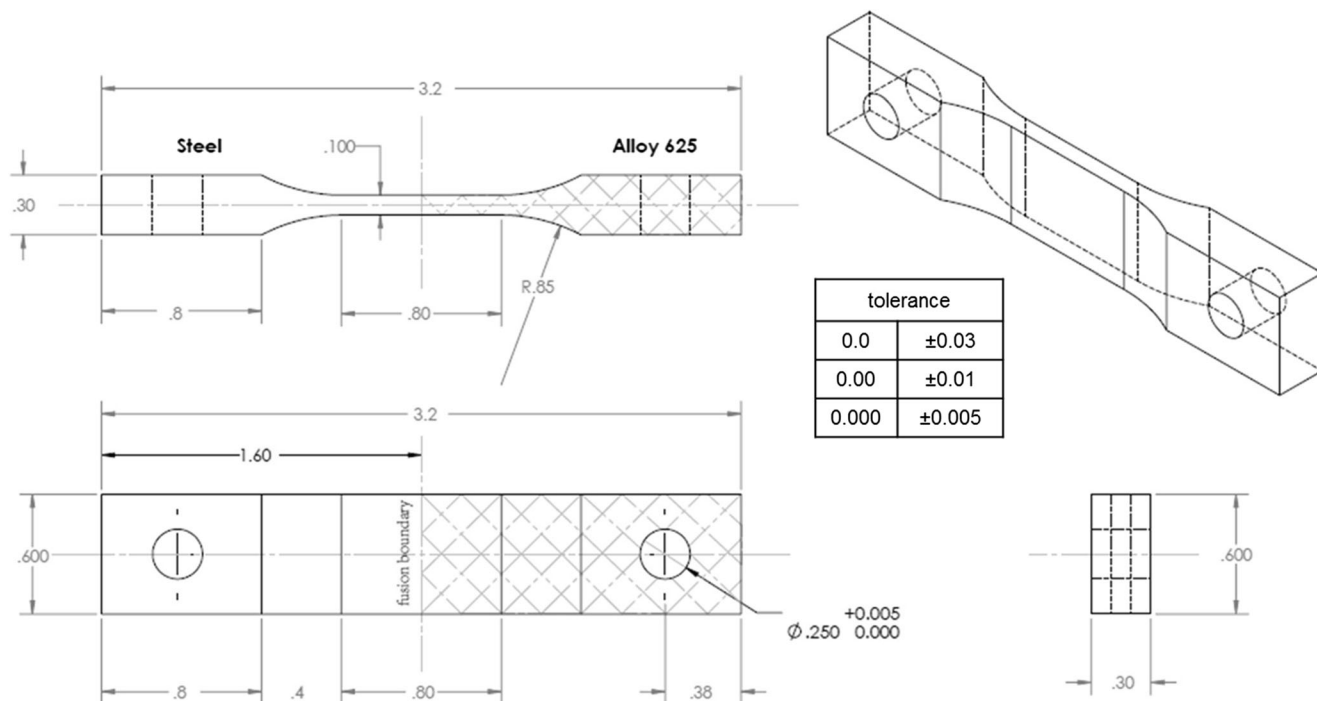

Fig. 2 Sample geometry for the DHCT with units in inches

Table 4 PWHT conditions of 8630/625 samples

Heat treatment	Temperature (°C)	Time (h)	HJP
HT-1	500	4	15,925
HT-2	550	4	16,955
HT-3	600	5	18,070
HT-4	620	6	18,555
HT-5	630	3.53	18,555
HT-6	640	6	18,970
HT-7	650	10	19,383
HT-8	660	10	19,593
HT-9	670	10	19,803
HT-10	660	50	20,154
HT-11	660	100	20,526

3 Results

3.1 Variation of time-to-failure with Hollomon-Jaffe parameter

DHCT results of the as-welded and 11 PWHT conditions are listed in Table 5. Note that with the exception of the 630 °C/3.5 h and 660 °C/100 h conditions, at least two samples were tested at each HJP. The time-to-failure (TTF) is an indicator of the HAC resistance and the location of fracture initiation is noted. The effect of the HJP on the HAC resistance can be easily seen by plotting the TTF versus HJP as shown in Fig. 4. In general, the TTF for all the samples was relatively short, less than 6 h in all cases. The shaded region in Fig. 4 shows the scatter in TTF which increases with higher HJP. Based on this tend curve, the optimal PWHT can be found in the HJP range ~ 18,500 to 19,500.

3.2 Fracture morphology after DHCT

The morphology of the fracture surfaces of 11 samples under different PWHT conditions are shown in Fig. 5. Only the fracture surface on the Alloy 625 side of the failure is shown. For each PWHT condition, the left-hand side image shows the macroscopic fracture surface with black lines as the boundaries separating regions with different fracture morphologies. In the right-hand side image, the regions with different fracture morphologies were color-coded to allow the relative proportions of different fracture types to be compared. The surface area of the different regions was measured with ImageJ and quantitatively compared among the 11 conditions to show the effect of PWHT on fracture morphology, as shown in the histograms in Fig. 6. In the following sections, the specific morphology of each region with a distinguishing color is described.

Fig. 3 **a** Overview of DHCT system. **b** loaded sample submersed in hydrogen charging solution. **c** Loading lever. **d** Hydrogen-charging circuit (courtesy of D. Bourgeois) [1, 6]
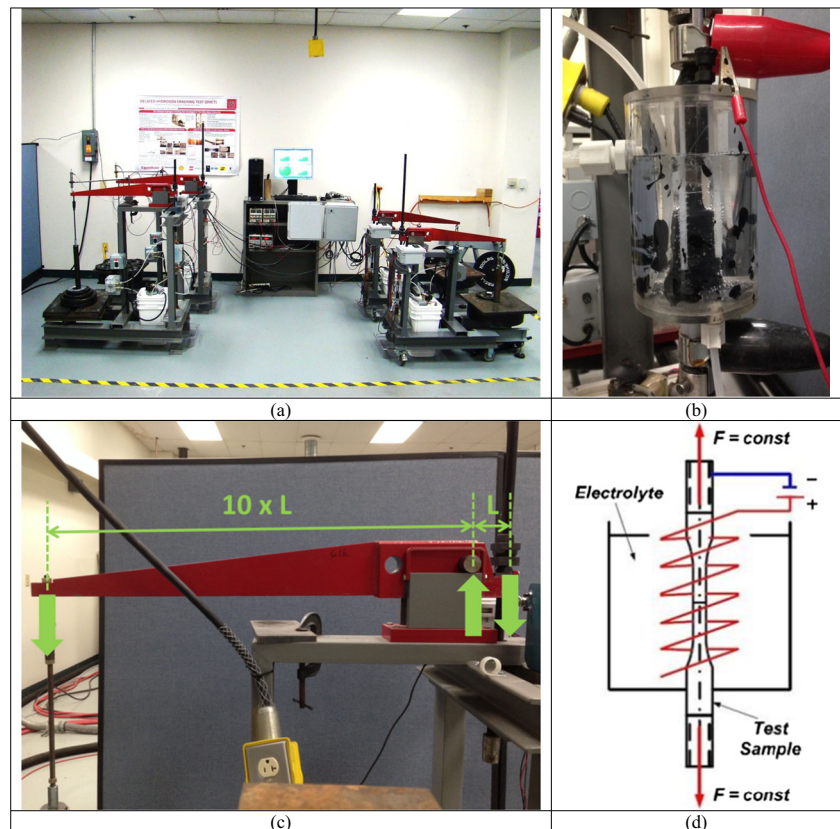
Table 5 DHCT results of 8630/625 samples in different PWHT conditions (CGHAZ coarse grain HAZ, PGZ planar growth zone)

| No. sample	PWHT	HJP	TTF (h)	Initiation location
1	As-welded	–	1.13	CGHAZ
2	As-welded	–	0.95	CGHAZ
3	500 °C/4 h	15,925	1.63	CGHAZ
4	500 °C/4 h	15,925	1.27	CGHAZ
5	500 °C/4 h	15,925	1.23	CGHAZ
6	550 °C/4 h	16,955	4.08	CGHAZ
7	550 °C/4 h	16,955	2.78	CGHAZ
8	600 °C/5 h	18,070	4.75	Fusion boundary or CGHAZ
9	600 °C/5 h	18,070	4.87	Fusion boundary or CGHAZ
10	620 °C/6 h	18,555	3.03	Fusion boundary
11	620 °C/6 h	18,555	2.52	Fusion boundary
12	630 °C/3.5 h	18,555	4.52	Fusion boundary
13	640 °C/6 h	18,970	2.48	Fusion boundary
14	640 °C/6 h	18,970	4.67	Fusion boundary
15	640 °C/6 h	18,970	5.7	Fusion boundary
16	640 °C/6 h	18,970	4.23	Fusion boundary
17	640 °C/6 h	18,970	2.47	Fusion boundary
18	650 °C/10 h	19,383	4.02	Fusion boundary
19	650 °C/10 h	19,383	5.38	Fusion boundary
20	650 °C/10 h	19,383	2.97	Fusion boundary
21	660 °C/10 h	19,593	2.8	Fusion boundary or PGZ
22	660 °C/10 h	19,593	3.15	Fusion boundary or PGZ
23	660 °C/10 h	19,593	5.9	Fusion boundary or PGZ
24	660 °C/10 h	19,593	4.22	Fusion boundary or PGZ
25	670 °C/10 h	19,803	3.62	Fusion boundary or PGZ
26	670 °C/10 h	19,803	5.92	Fusion boundary or PGZ
27	670 °C/10 h	19,803	1.73	Fusion boundary or PGZ
28	660 °C/50 h	20,154	1.75	PGZ
29	660 °C/50 h	20,154	3.42	PGZ
30	660 °C/100 h	20,526	1.48	PGZ
31	660 °C/100 h	20,526	2.83	PGZ
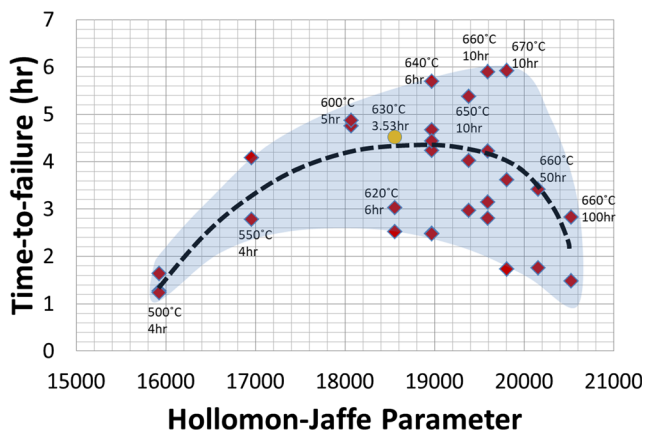
Fig. 4 Summary of the DHCT results and the trend line of TTF with respect to HJP

3.2.1 Purple region - quasi-cleavage in CGHAZ

The "purple" regions of the fracture are observed in the samples in the untempered or slightly tempered conditions, i.e., as-welded, 500 °C/4 h, 550 °C/4 h, and 600 °C/5 h conditions, as shown in Fig. 6a. These correspond to the fracture surface through the CGHAZ. Figure 7 shows the typical morphologies of the purple regions under different conditions. For the as-welded condition, the morphology is typically quasi-cleavage with radial "river markings" as the propagation paths of the fracture. The radiant center of the "river markings" is believed to be the crack initiation site, which is in the martensitic CGHAZ (Fig. 7a). The purple regions in the slightly tempered conditions 500 °C/4 h, 550 °C/4 h, and 600 °C/5 h are greatly reduced (Fig. 5b–d) relative to the as-welded condition. The area decreases with HJP increase, except the PWHT at HJP = 18,070 in Fig. 6a, maybe because of the inhomogeneity of the base metal or

abnormal in the dynamic process of fracture propagation. Figure 7b–d also shows fracture morphologies of low energy and high brittleness, with martensitic lath structure features. The fracture morphology is believed to be the initiation site of the HAC. Both visual observation and EDX analysis indicate that the purple regions represent the fracture through the CGHAZ.

3.2.2 Green region - microvoid coalescence in weld metal

All the fracture surfaces in Fig. 5 contain "green" regions. At higher magnification, all these green regions appear similar and three representative photos of fracture morphology are shown in Fig. 8. The fracture morphology

(a)

(b)

(c)

(d)

(e)

(f)
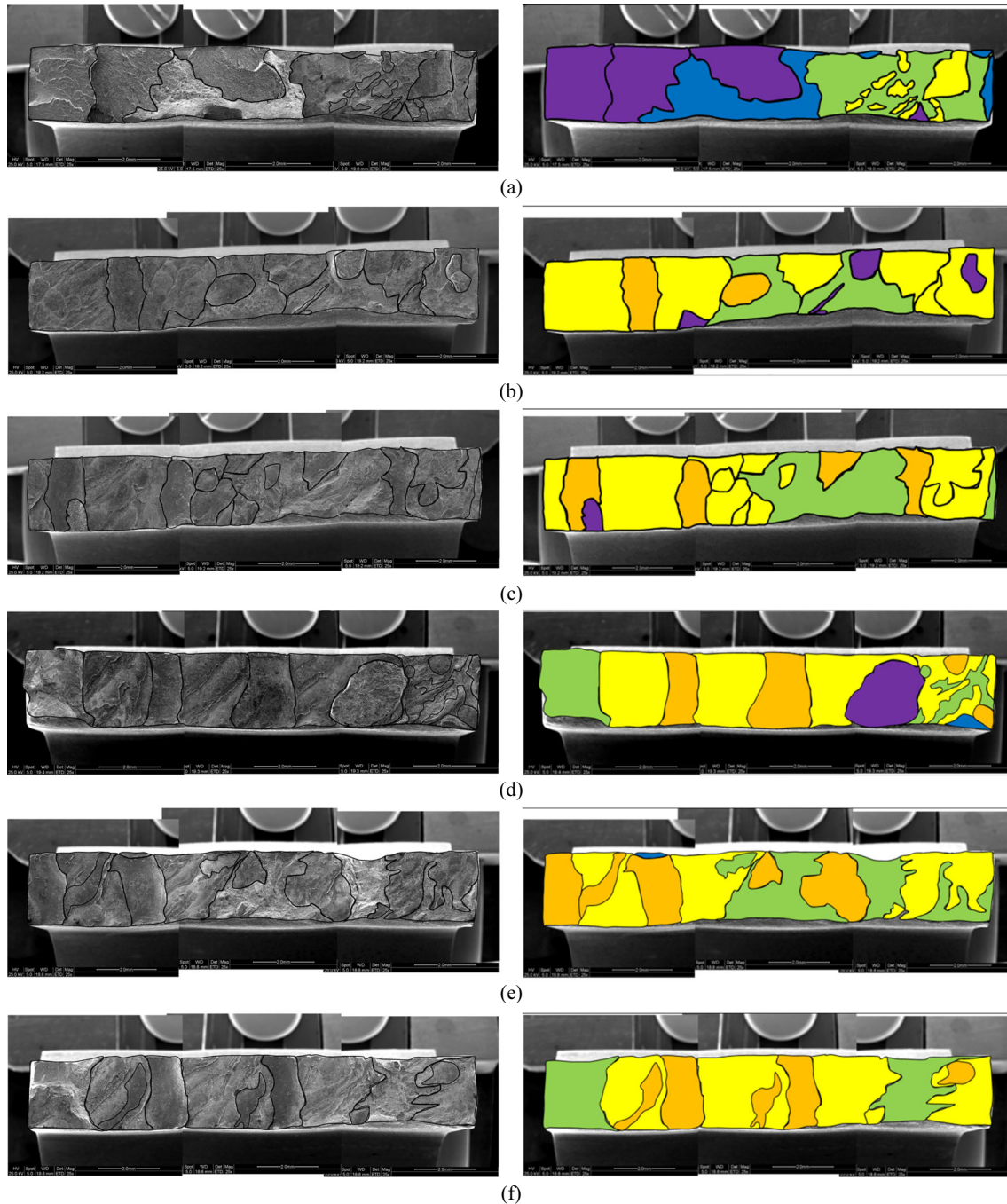
Fig. 5 Fracture behavior of 11 PWHT conditions after failure in the DHCT. **a** As welded, **b** 500 °C/4 h, **c** 550 °C/4 h, **d** 600 °C/5 h, **e** 620 °C/6 h, **f** 640 °C/6 h, **g** 650 °C/10 h, **h** 660 °C/10 h, **i** 670 °C/10 h, **j** 660 °C/50 h, **k** 660 °C/100 h. Different fracture morphologies are represented by different colors. Purple = quasi-cleavage in CGHAZ, orange = fusion boundary fracture, yellow = fusion boundary fracture with complex transition features, light green = microvoid coalescence in weld metal by overload, scarlet = terrace fracture or cleavage fracture in PGZ, blue = overload fracture in base metal
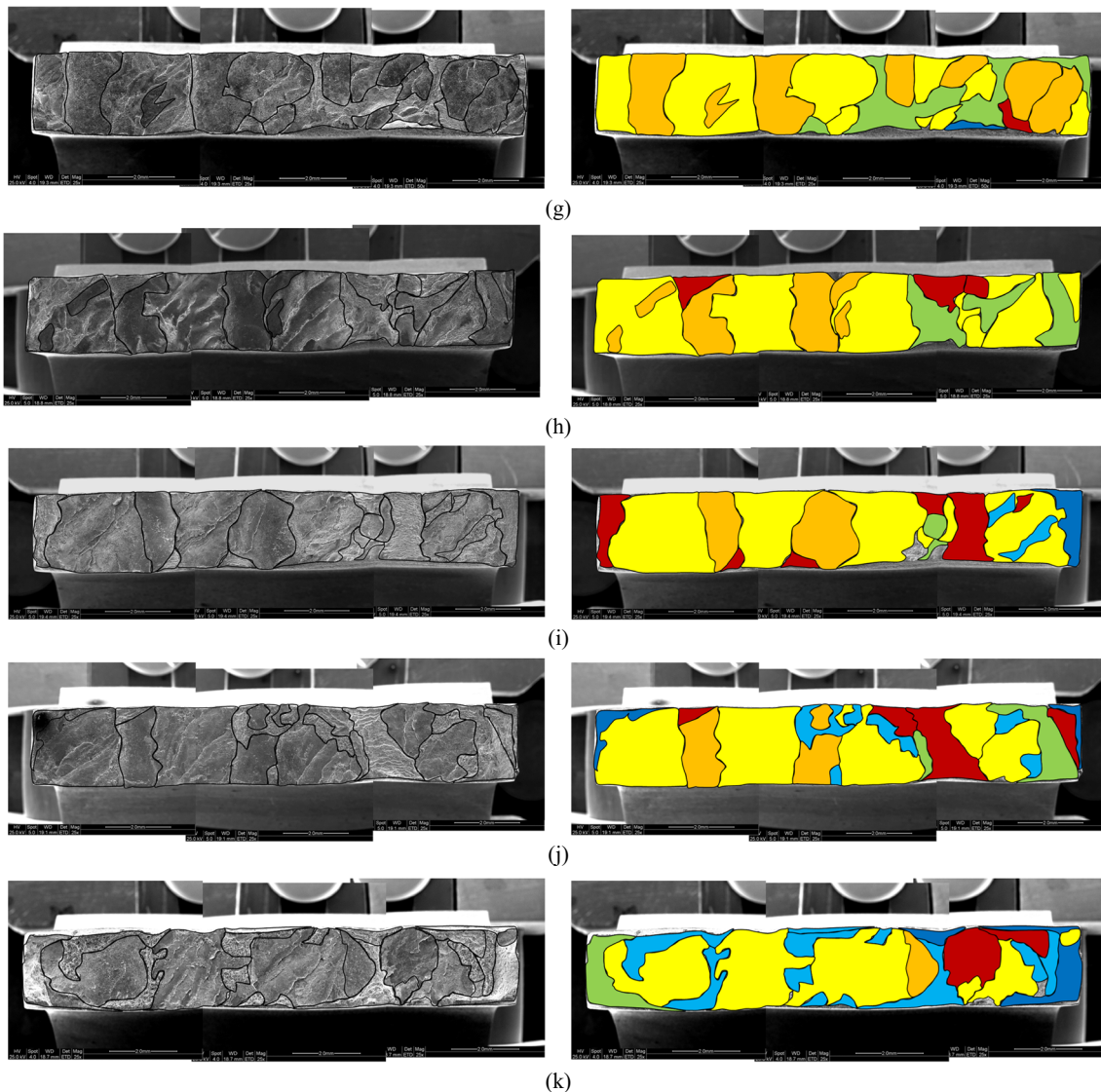
(g)

(h)

(i)

(j)

(k)

Fig. 5 (continued)

is classical ductile, microvoid coalescence (MVC) with propagation through the weld metal near the fusion boundary, as verified using the EDX analysis (Fig. 8b). The green region fracture results from overload since the crack propagates through the weld metal that has lower strength than the CGHAZ, fusion boundary, or PGZ. In the first five PWHT conditions, precipitation hardening in the weld metal was probably not strong. The fracture in these samples tended to propagate through the weld metal with the "green" fracture region representing 20–30% of the entire fracture surface (Fig. 6e). Since the Alloy 625 weld metal is an FCC crystal structure and not favorable for hydrogen diffusion compared to base metal, it is believed that the "green" region results from overload or fracture propagation without hydrogen assistance. In as-welded condition, the "green" area percentage is 25.1%.

In this sample (Fig. 5a), the fracture initiated in the CGHAZ and propagated mainly through the CGHAZ and the weld metal (green region).

3.2.3 Orange region - fusion boundary fracture

All the fracture surfaces of PWHTed samples contain "orange" region. Only the as-welded condition did not exhibit this fracture morphology. This region represents the fracture surface along the fusion boundary. As shown from Fig. 6c, the area percentage of this fracture type increases and then decreases, similar to the trend of time-to-failure of the DHCT in Fig. 4.

SEM images of "orange" fracture in Fig. 9 show that the morphology is flat and relatively smooth. The "white boundaries" in Fig. 9a are commonly but not always observed on the fracture surface. When the weld metal and base metal
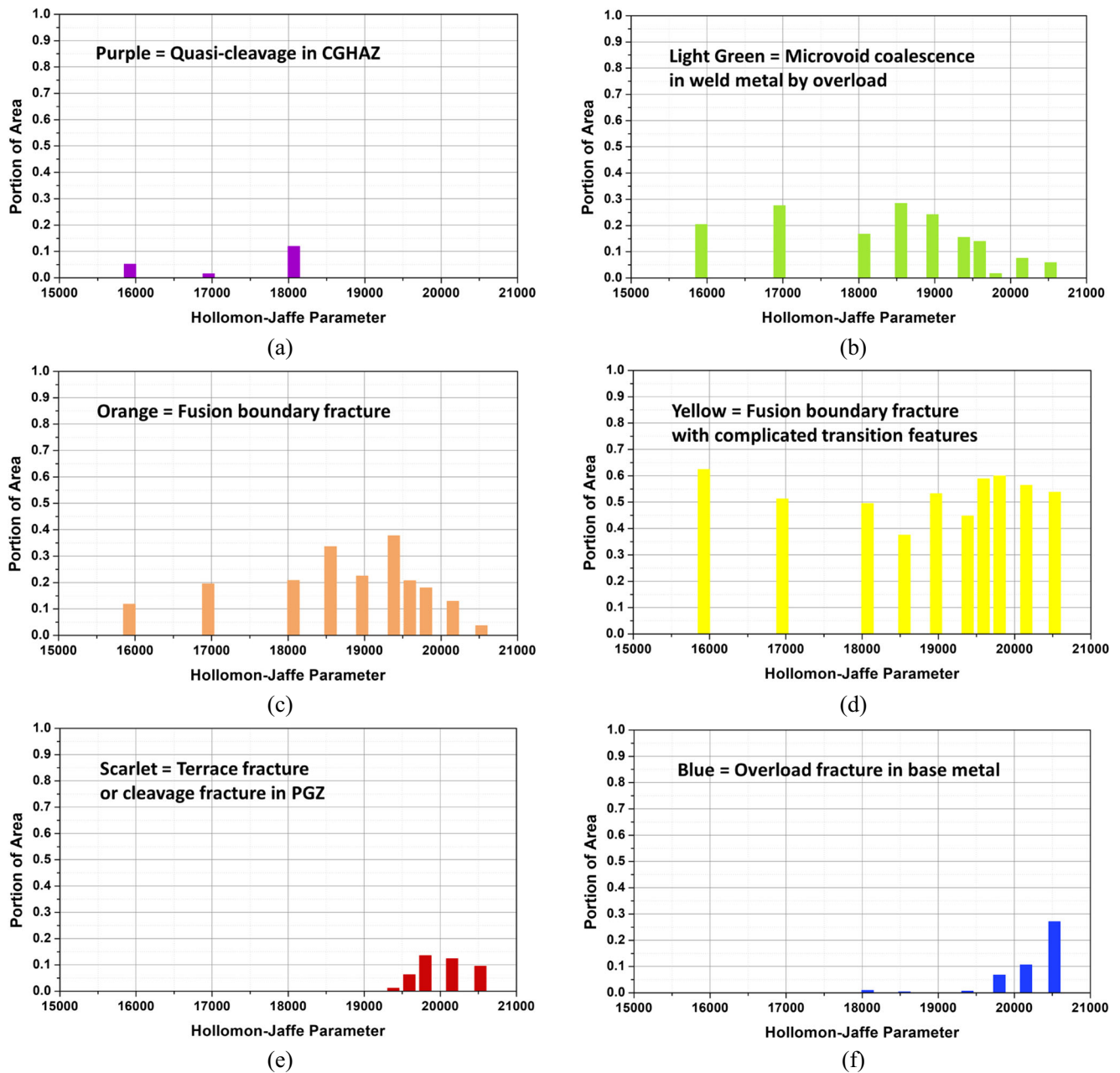
Fig. 6 The area percentage of the color-coded fracture morphology as a function of HJP

separated along the fusion boundary, the weld metal penetrating into base metal grain boundaries was pulled out from the base metal grain boundaries and left on the fracture surface on the weld metal side. The EDX analysis verified that the "white boundary" contains higher content of nickel and lower iron than the region just adjacent to the boundary (Fig. 9b).

Figure 9c–d shows the fracture surface without "white boundaries". The fracture surface of Fig. 9c is so smooth that it probably resulted from brittle HAC. For the PWHT condition 670 °C/10 h, part of the PGZ was pulled out and part of the base metal was left on the fracture surface as

shown in Fig. 9d. This image verifies that the fracture is definitely along the fusion boundary, rather than through the PGZ or base metal. Interestingly, when the sample was tempered at 670 °C/10 h or higher HJPs, precipitates started to appear on the fracture surfaces, as shown in Fig. 9f (660 °C/50 h) and h (660 °C/100 h). Some of the precipitates separated from the fracture surface and left the holes. Thus, both the precipitates and holes can be observed in Fig. 9f and h. These precipitates probably promoted HAC at the interface between the precipitates and the matrix, since this interface is a strong hydrogen trap.

Fig. 7 Fracture morphology of the "purple" region in different PWHT conditions. **a** as-welded from Fig. 5a. **b** 500 °C/4 h from Fig. 5b. **c** 550 °C/4 h from Fig. 5c. **d** 600 °C/5 h from Fig. 5d

(a)

(b)

(c)

(d)
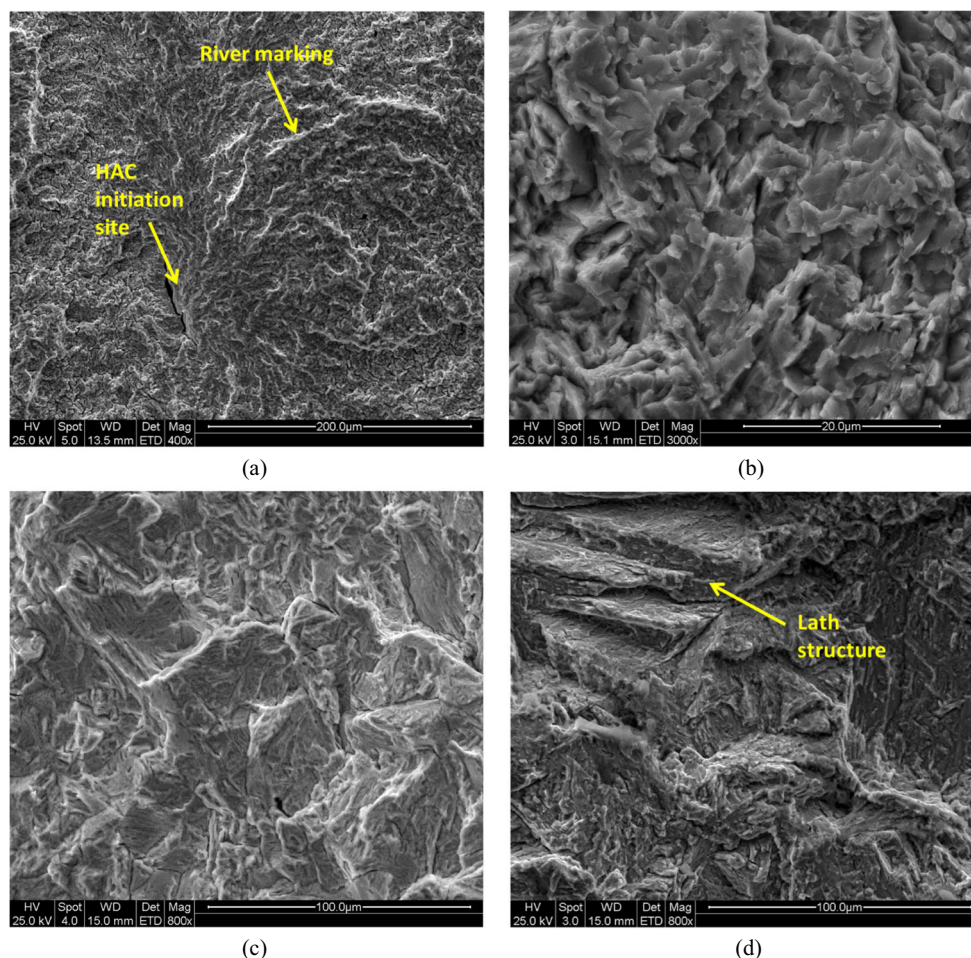
3.2.4 Yellow region - fusion boundary fracture with transition features

The morphology represented by "yellow" regions is found in all PWHT conditions (Fig. 5). Figure 10 shows a closer view of the fracture surfaces, which contain many smaller fracture features along the fusion boundary and the transition regions. The fracture through the transition region represents the swirl patterns or the diluted weld metal region as indicated in EDX analysis with high iron content. The diluted weld metal region contains fresh martensite with high hardness and fracture in this region probably result from HAC. When the HJP is high enough, such as 660 °C/50 h in Fig. 10d–e, the fracture propagated along the boundary between the PGZ and the cellular solidification region in the weld metal. The small protuberances on the order of 5–10 μm probably represent the change from planar to cellular growth in the transition region (Fig. 10e). For high HJP PWHT conditions, carbon can diffuse through the PGZ (less than 10 μm in width) and form carbides near the boundary between the PGZ and the cellular-grain region, as reported in a previous paper [2]. Thus, HAC in the "yellow" regions tends to occur along the boundary between the PGZ and the cellular-grain region. This HAC fracture behavior

occupies a large area percentage in all the PWHT conditions, as shown in Fig. 6d. By inference from the river lines resulting from fracture transition and relatively rough features on the fracture surfaces, the HAC probably propagated through the "yellow" regions but did not initiate in these regions.

3.2.5 Blue region - overload fracture in base metal

The morphology represented by "blue" regions appears in the as-welded condition and in PWHT conditions 600 °C/5 h, 620 °C/6 h, 650 °C/10 h, 670 °C/10 h, 660 °C/50 h, and 660 °C/100 h, and consists of overload fracture. The as-welded sample in Fig. 11a contains a large area percentage of the "blue" morphology. The morphology is quite different from the hydrogen-assisted fracture through the CGHAZ in Fig. 7 (purple region), because it propagated through the CGHAZ due to overload rather than the HAC.

In samples with high HJP, the "blue" regions also result from overload but appear quite different from the as-welded condition as shown in Fig. 11b–e. Figure 11b shows an image with both the fracture along fusion boundary (orange) and the dimple fracture (blue). The "blue" region definitely propagated through the base metal HAZ based on the abrupt shift to ductile rupture

Fig. 8 Fracture morphology in the "green" regions. **a** As-welded sample, from Fig. 5a. **b** EDX analysis spectrum of the red circle in Fig. 8a. **c** Sample 660 °C/10 h, from Fig. 5h. **d** Sample 660 °C/50 h, from Fig. 5j

(a)

(b)

(c)

(d)
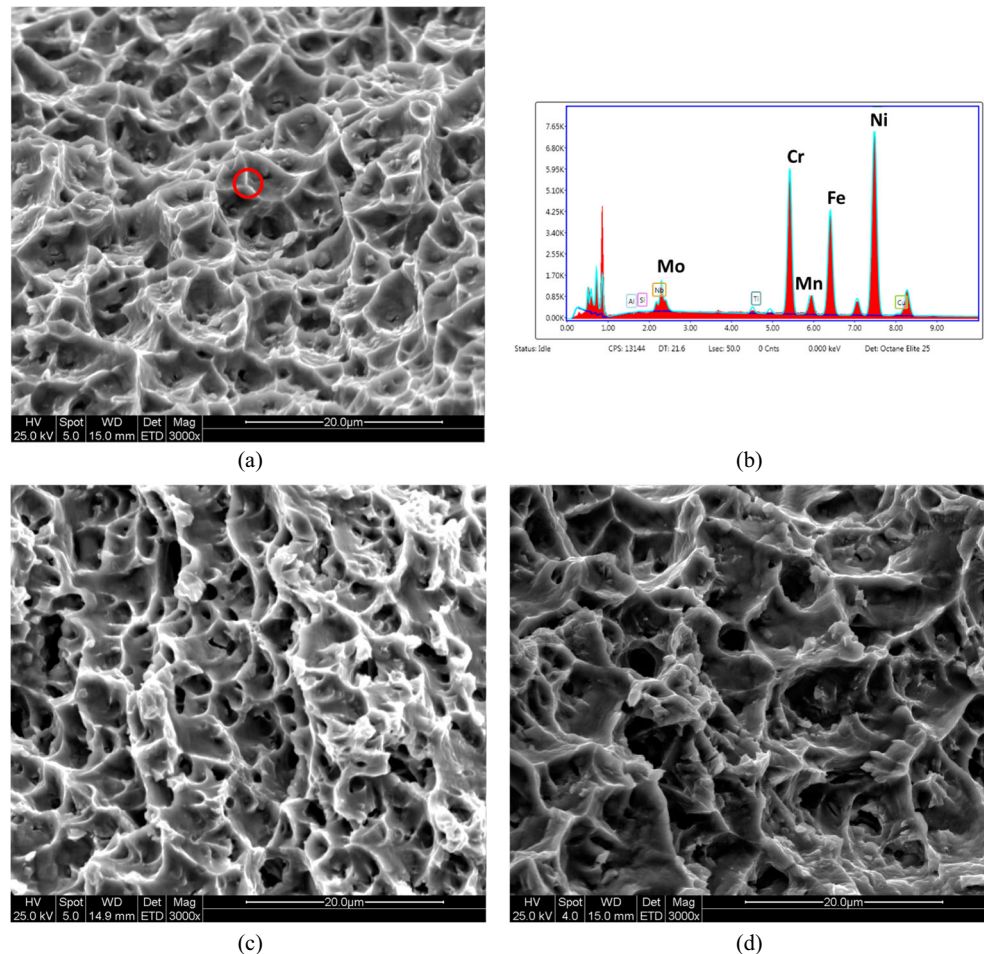
features. Figure 11c also shows an image with both "orange" (left) and "blue" regions but the morphology of the "blue" region is different from that in Fig. 11b. The EDX mapping verified the "blue" region contains mainly iron and it is through the base metal. Figure 11e shows the "blue" region of the sample at 660 °C/100 h. The fracture contains a mixture of quasi-cleavage and ductile dimple morphologies. The EDX analysis revealed that the fracture is through the base metal. The fracture morphology in Fig. 11e resembles quasi-cleavage HAC morphology described by Beachem [26], but the CGHAZ after PWHT 660 °C/100 h is almost entirely ferrite [2]. Thus, the fracture morphology results from overload instead of HAC.

3.2.6 Scarlet region - terrace fracture or cleavage fracture in PGZ

The morphology represented by the "scarlet" regions appears in Fig. 5g–k. In this region, the fracture propagated into the PGZ from the fusion boundary surface because carbides started to form after sufficient carbon pile up [2, 10, 11], such as in condition 650 °C/10 h or higher HJP conditions. The cliff and valley morphology through the PGZ from the fusion boundary to the weld metal formed due to HAC (Fig. 12).

The area percentage of the "scarlet" region is more than 10% for samples 670 °C/10 h, 660 °C/50 h, and 660 °C/100 h. Sample 660 °C/100 h also contains quasi-cleavage morphology through PGZ fracture as described below.

The fracture surface of sample 660 °C/100 h exhibits a brittle quasi-cleavage morphology through the PGZ. This fracture morphology represents a typical initiation site of HAC [29] (Fig. 13a, b). The EDX mapping confirmed that the quasi-cleavage fracture is through the PGZ and also showed that the fusion boundary surface contains much higher iron than the PGZ (Fig. 13c, d).

4 Discussion

4.1 Relationship between the Hollomon-Jaffe parameter and HAC susceptibility

The DHCT results reveal that the HAC susceptibility of the 8630/625 DMW in ambient temperature is a function of the HJP, but not as a strong function as that of F22/625 DMW reported previously [1]. The time-to-failure (TTF) results of 8630/625 samples in this work and the TTF of F22/625

Fig. 9 Examples of "orange" fracture behavior. **a** 550 °C/4 h, from Fig. 5c showing "white boundaries". **b** EDX line scan across the "white grain boundaries" in the framed area in Fig. 9a. **c** 660 °C/10 h, no "white grain boundaries". **d** 670 °C/10 h, with the exposed PGZ and residual base metal. **e** 660 °C/ 50 h. **f** Precipitates on fracture surface of sample 660 °C/50 h in the framed region. **g** 660 °C/ 100 h. **h** The precipitates on fracture surface of sample 660 °C/ 100 h in the framed region
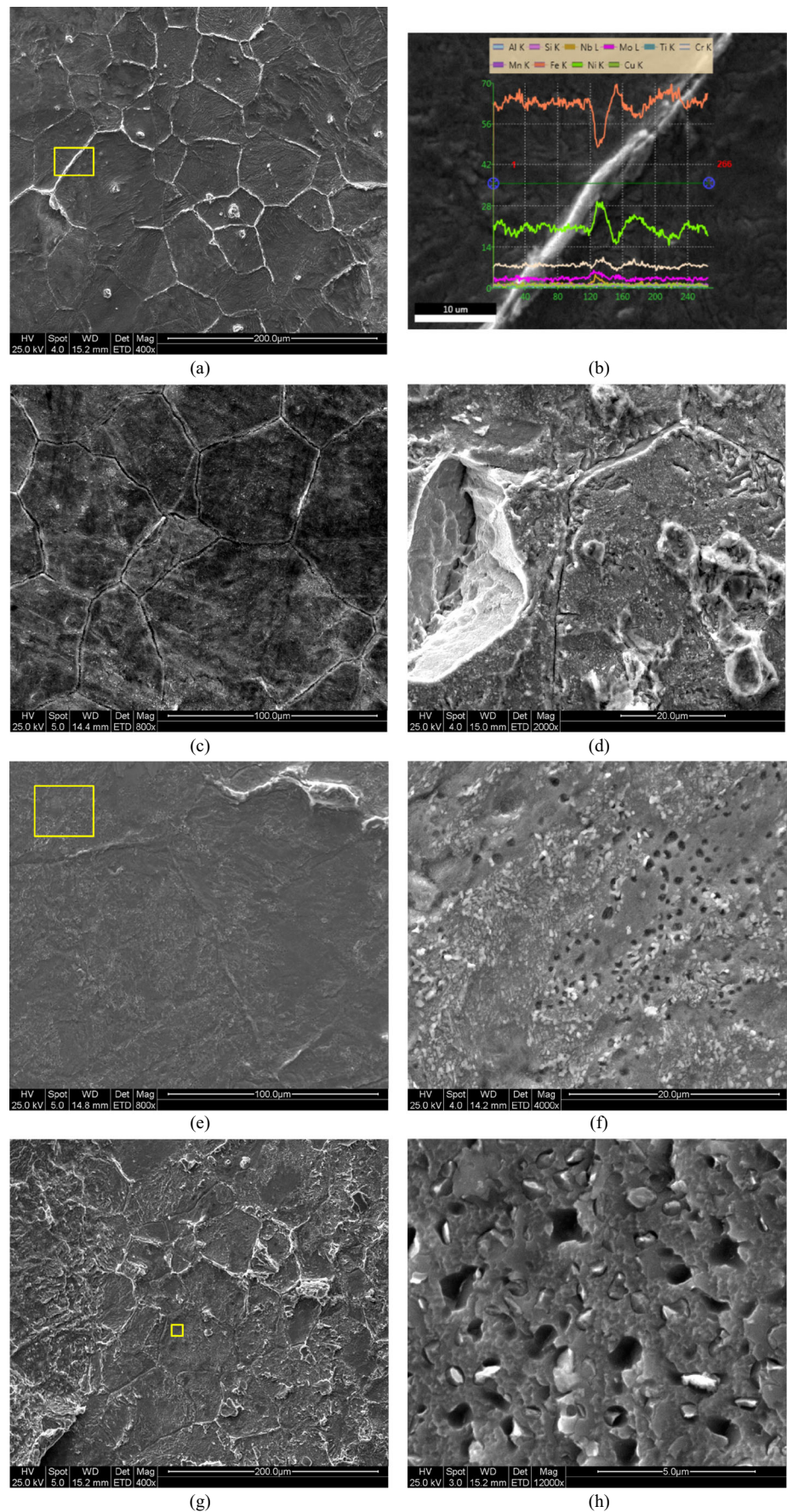
Fig. 10 Typical fracture morphology of the "yellow" regions in selected PWHT conditions. a 550 °C/4 h, from Fig. 5c. b 660 °C/10 h, from Fig. 5h. c EDX analysis spectrum of the red circle in Fig. 10b. d 660 °C/50 h, from Fig. 5j. e 660 °C/50 h, from Fig. 5j, the protuberance features on fracture along the boundary between the PGZ and the cellular solidification growth region. f 660 °C/100 h, from Fig. 5k
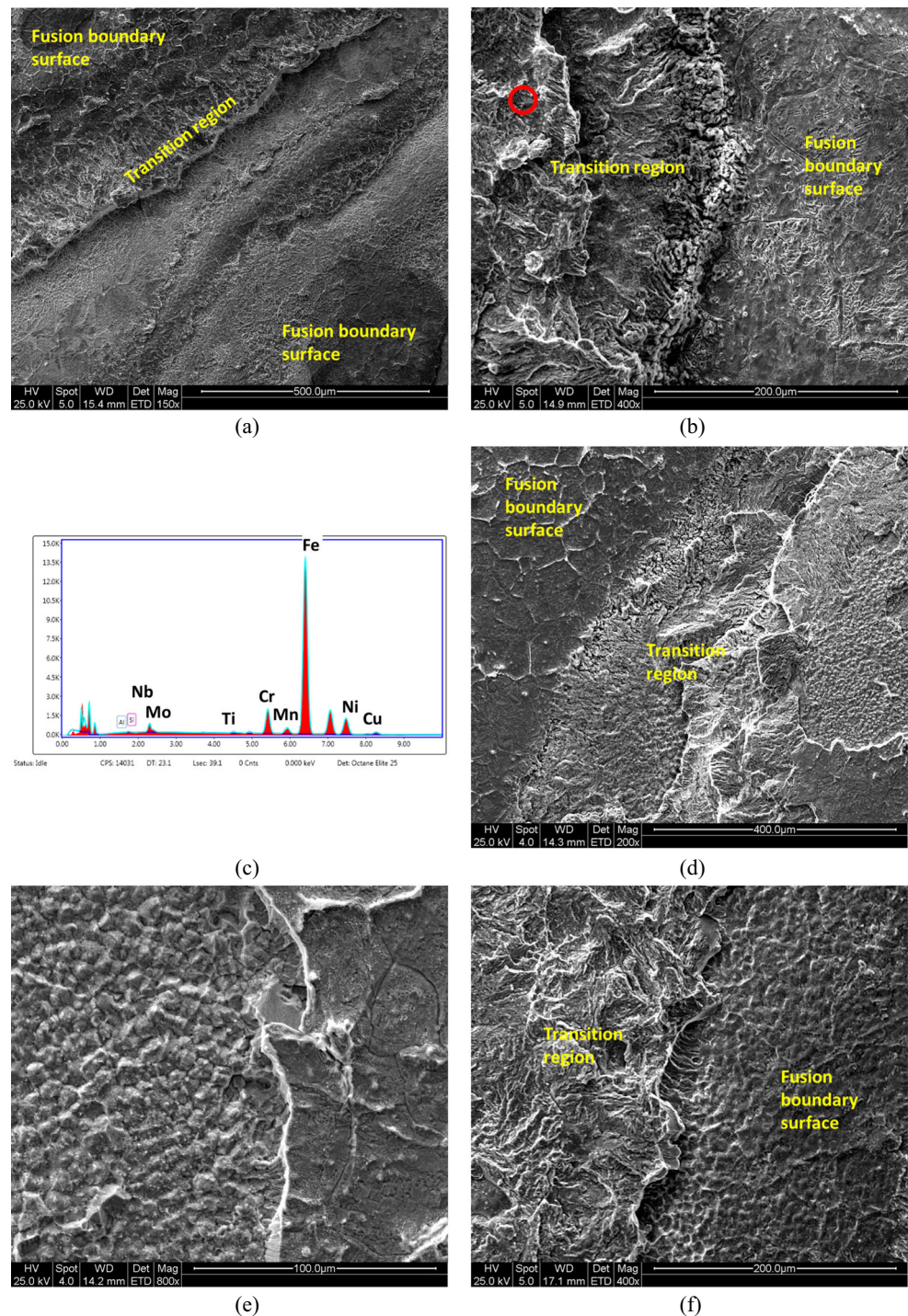
DMW are compared in Fig. 14. Generally, the TTF of 8630/625 samples is far shorter than the F22/625 samples and thus more susceptible to HAC than the F22/625 samples. It should be noted that the applied stress for the 8630/625 samples was 40 ksi, smaller than the 61 ksi used in DHCT of F22/625 samples. Also, the sulfuric acid solution for 8630/625 samples had a pH = 1.74 ± 0.02, slightly higher than that of F22/625, pH = 1.29 ± 0.02. Thus, the solution used for the 8630/625 samples probably generates

less hydrogen, and overall, the testing conditions were not as severe as those used for F22/625.

Over a wide range of HJP from 16,000 to 20,500, the trend curve of the TTF is flatter than that of F22/625 DMW samples. According to the purple trend curve in Fig. 14, there is not a clear peak of TTF for 8630/625 DMW as there is for the F22/625 DMW. For the 8630/625 samples, maximum TTF is in the HJP = 18,500~19,500, smaller than that of F22/625 samples (HJP = ~20,000). The difference between 8630/625

Fig. 11 Typical fracture morphology of the "blue" regions in selected samples. **a** As-welded, from Fig. 5a. **b** 670 °C/10 h, from Fig. 5i. **c** 660 °C/50 h, from Fig. 5j. **d** EDX mapping of the fracture area in Fig. 11c. **e** 660 °C/100 h, from Fig. 5k. **f** EDX point analysis of the red circle in Fig. 11e
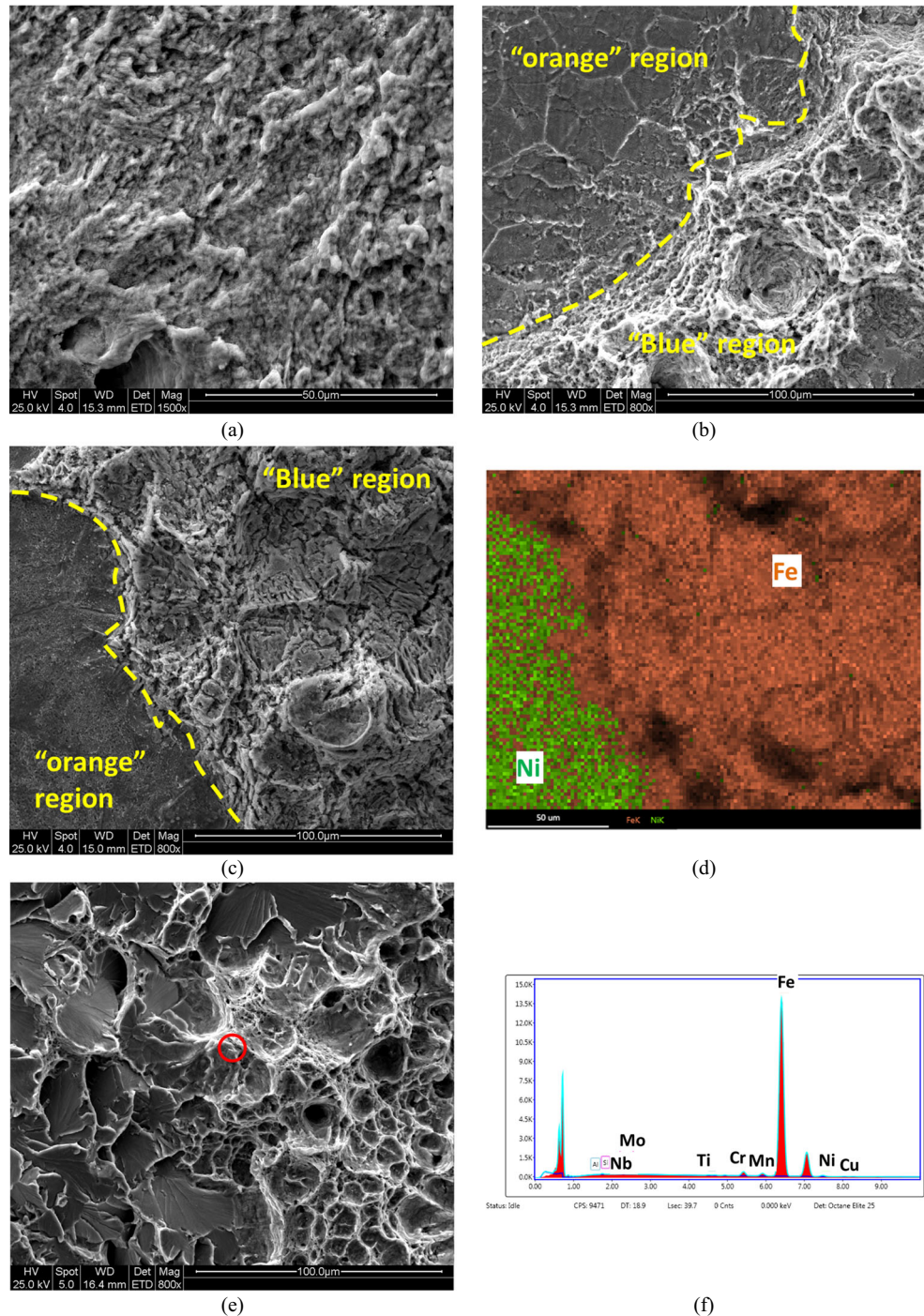

samples and F22/625 samples shown in Fig. 14 is similar to the results of the three-point bend hydrogen cracking test reported by Dodge [11].

In the range HJP < 19,800, the CGHAZ hardness of the 8630/625 samples is about 40–70 VHN higher than that of the F22/625, as reported in a previous paper [2]. Also, the PGZ hardness of 8630/625 samples increases at a higher rate with regard to HJP relative to the F22/625 samples [2]. This reflects the higher carbon content of the 8630 steel and the resultant rapid pile up of carbon at the PGZ.

The change in hardness of the CGHAZ, PGZ, and weld metal as a function of HJP for the 8630/625 samples is shown in Fig. 16. As expected, the CGHAZ hardness decreases with HJP but does not drop below 250 VHN until the HJP exceeds 19,750. Thus, meeting the NACE requirement of < 250 VHN requires quite severe PWHT conditions. Below an HJP of

Fig. 12 Typical morphology of the "scarlet" region fracture in selected PWHT conditions. **a** 660 °C/10 h, from Fig. 5h. **b** 670 °C/10 h, from Fig. 5i. **c** 660 °C/50 h, from Fig. 5j. **d** 660 °C/100 h, from Fig. 5k
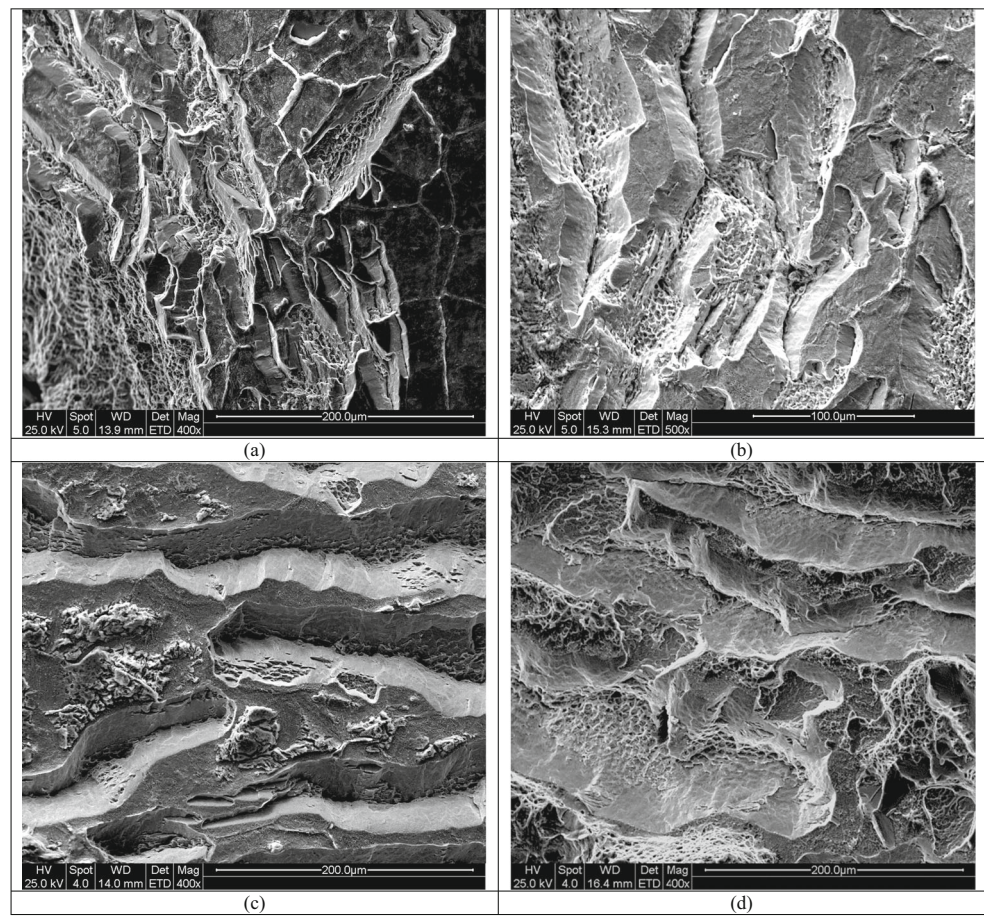
19,000, there is little change in the PGZ and weld metal hardness. Above 19,000 HJP, the PGZ hardness increases dramatically, and under extreme PWHT conditions reaches hardness levels exceeding 550 VHN. The blue-shaded band running from 18,500 to 19,500 HJP (Fig. 15) represents the PWHT conditions that maintain the hardness in all three regions below 350 VHN and corresponds to the longest TTF seen in the 8630/625 samples.

Because the PGZ hardness of 8630/625 samples increases at a much higher rate with HJP than F22/625 samples [2], the HAC resistance (TTF) of 8630/625 samples starts to decrease at smaller values of HJP. Thus, the HJP "sweet spot" of 8630/625 for maximum TTF must be smaller than F22/625 samples. The purple TTF trend curve of 8630/625 samples is on the left of the trend curve of F22/625 samples (Fig. 14). This is primarily due to the higher carbon content of 8630 that results in more rapid embrittlement of the PGZ.

Based on Fig. 15, it is difficult to identify an optimal HJP range for the 8630/625 samples only based on hardness TTF since there is no range of HJP in which the CGHAZ hardness decreased to ≤ 250 VHN and the PGZ hardness remains relatively low (≤ 300 VHN). In contrast, the F22/625 samples exhibit an optimal PWHT range

between 19,750 and 20,250 HJP where the CGHAZ hardness is < 250 VHN and the PGZ and weld metal hardness do not exceed 300 VHN [1]. This observation confirms why the HAC resistance of 8630/625 is so low in practice, particularly if PWHT reduces the CGHAZ hardness to below 250 VHN. In practice, it is impossible to achieve the CGHAZ hardness < 250 VHN without embrittling the PGZ at the weld interface.

4.2 Fractography

Six fracture morphologies were identified in failed DHCT samples of the 8630/625 DMW. The fracture morphologies of the "green" and "blue" resulted from overload rather than HAC. Similar fracture morphology resulting from overload was also found in failed samples of the F22/625 DMW [1]. The other four typical fracture morphologies (refer to Fig. 5) are associated with hydrogen. Based on the fractography work, a sketch summarizing a cross-section view of the fracture path is shown in Fig. 16. The parentheses with different colors represent the corresponding color-coded fracture regions described previously.

In the HJP range $< 18,500$, the HAC tends to initiate and propagate in the tempered martensite in the CGHAZ, forming

Fig. 13 The morphology of a "scarlet" region in the sample 660 °C/100 h, from Fig. 5k. **a** Overview. **b** Higher magnification of the area in white frame in Fig. 13a. **c** Higher magnification of the area in yellow frame in Fig. 13a. **d** EDX mapping of the fracture area in Fig. 13c
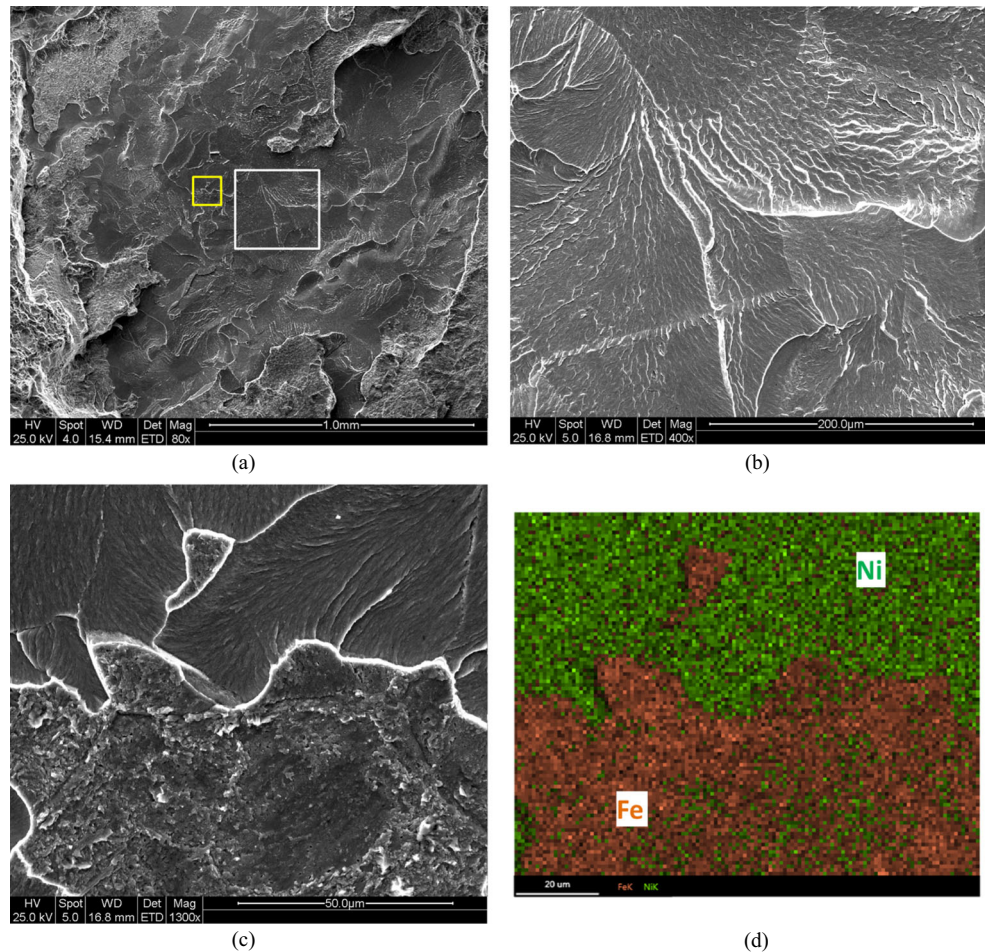
the fracture morphologies in the "purple" regions. In the HJP range ~ 19,500, the HAC tends to initiate in the PGZ due to the precipitation of M_7C_3 carbides [2, 10, 11], as shown in the fracture morphologies in the "scarlet" regions. In the HJP range ~ 19,800, precipitates were found on the fusion boundary surface ("orange" regions) and the HAC probably initiates due to these precipitates. For the HJP range > 19,800, there are

two types of possible HAC initiation sites and the TTF should decrease quickly.

The fractography work reveals that the most susceptible microstructures to HAC initiation are the martensitic CGHAZ ("purple" region in Fig. 7) and the PGZ after strong PWHT ("scarlet" region in Figs. 12 and 13). In the diagram of area percentages of the two color-coded

Fig. 14 Comparison of the time-to-failure between the 8630/625 samples and F22/625 samples. The green square points and purple trend curve are for 8630/625 samples, and the scarlet diamond points and black trend curve are for F22/625 samples [1]
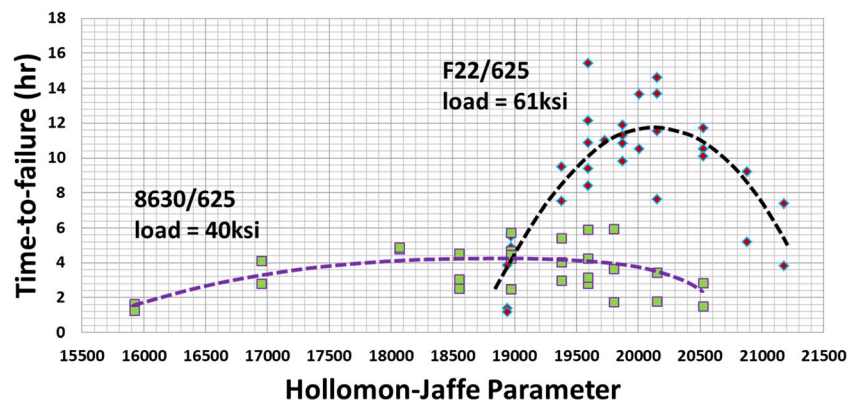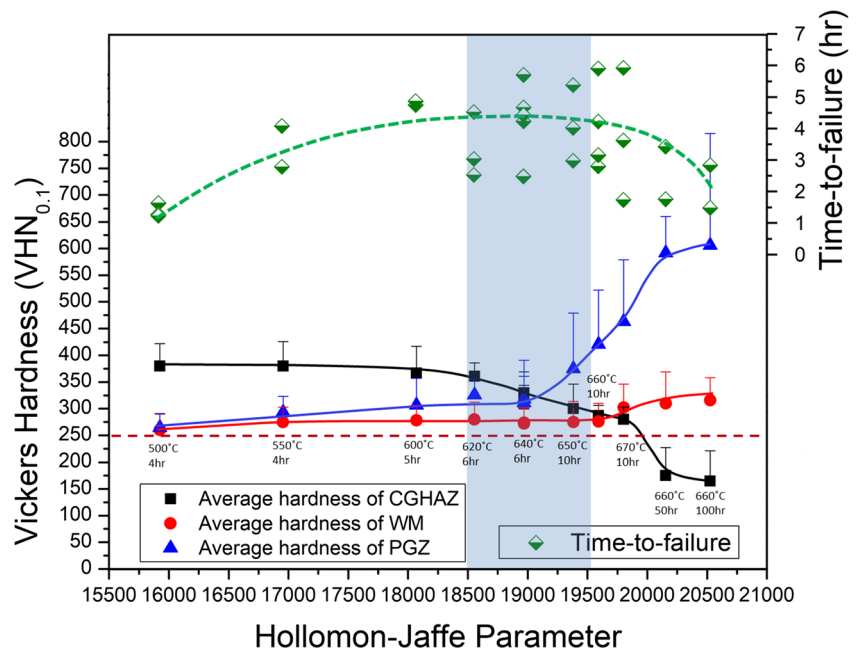
Fig. 15 The time-to-failure variation and hardness variation of 8630/625 samples with HJP [2]

regions, the HJP range from 18,500 to 19,500 contains little of the most susceptible "purple" and "scarlet" fracture. The area percentage of the susceptible fracture surfaces also confirmed that the optimal HJP range is 18,500–19,500 (Fig. 17).

Figure 6b shows that the area percentages of "green" regions are similar among the first five PWHT conditions. Starting from the sixth condition, the area decreases with the increase in HJP. This is consistent with the hardness

change of the weld metal as shown in Fig. 15, in which the weld metal hardness does not start to increase until the PWHT 660 °C/10 h (HJP = 19,593). At higher values of HJP, precipitation hardening results in a rapid increase in weld metal hardness.

The "yellow" region formed due to fracture propagation assisted by hydrogen and it was not found in failed DHCT samples of F22/625 DMW [1]. The microvoid coalescence (MVC) fracture through base metal was found
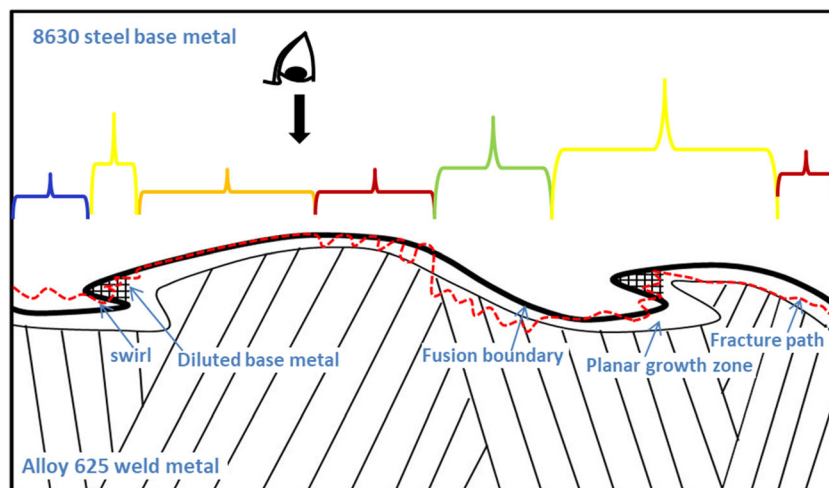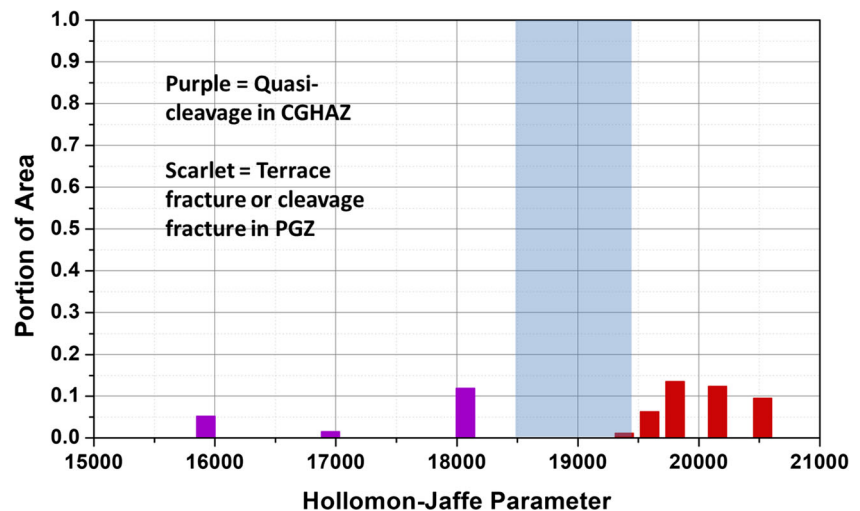

Fig. 16 A sketch of the side view of the fracture path and the typical fracture regions indicated by parentheses with different colors, corresponding to different color-coded regions. The sketched eye means that the fracture surface was observed in this direction under SEM. Different colors represent different fracture morphologies. Blue = overload fracture in base metal, yellow = fusion boundary fracture with complex transition features, orange = fusion boundary fracture, scarlet = terrace fracture or cleavage fracture in PGZ, light green = microvoid coalescence in weld metal by overload.

in failed samples of the F22/625 DMW but not in the 8630/625 DMW [1]. In the HJP range < 19,800, the CGHAZ hardness of F22/625 samples is lower than that of the 8630/625 samples at the same PWHT. For the F22/625 DMW, the fracture tended to propagate through the CGHAZ (base metal) with a MVC morphology, consuming higher fracture energy [1]. However, assisted by hydrogen, the fracture of the 8630/625 DMW tended to propagate along the fusion boundary and through the diluted weld metal region [2], resulting in a brittle fracture morphology (yellow) with lower fracture energy.

Among the PWHTed samples, the "blue" regions are mainly present in samples with high HJP (670 °C/10 h, 660 °C/50 h, and 660 °C/100 h) with the area percentage increases with the HJP (Fig. 6f). At 670 °C/10 h or more extreme PWHT, the average CGHAZ hardness decreases below that of the weld metal and the PGZ (Fig. 15) due to carbon depletion [2]. The fracture tended to propagate through the region with the lowest hardness, namely the lowest strength. Therefore, the area percentage of the "blue" fracture increased (Fig. 7f–h).

5 Conclusions

This investigation has shown the influence of PWHT on the hydrogen-assisted cracking behavior of 8630/625 dissimilar metal weld samples using delayed hydrogen cracking tests. The PWHT range was determined within which the HAC resistance is optimal. Fractography work revealed the variation of fracture morphology and HAC initiation location with the PWHT. Specific conclusions are listed below.

1) The delayed hydrogen cracking test (DHCT) revealed that HAC resistance (indicated by time-to-failure) of the 8630/625 samples is relatively low. In the same hydrogen charging and loading system, 8630/625 samples are more

susceptible to HAC than F22/625 samples with similar PWHT conditions.

2) Based on the DHCT results, hardness testing and fractography, the optimal HJP range for the 8630/625 DMW is 18,500 to 19,500. This HJP range included the following PWHTs studied in this work: 620 °C/6 h, 640 °C/6 h, and 650 °C/10 h.

3) Under "optimal" PWHT conditions (highest TTF), the hardness of both the CGHAZ and planar growth zone (PGZ) was in the range from 300 to 350 VHN.

4) Under PWHT conditions that reduced the CGHAZ hardness to below 250 VHN, the PGZ hardness exceeded 550 VHN and TTF in the DHCT was reduced.

5) Six distinct fracture morphologies were identified. Four fracture morphologies are associated with HAC and two occur due to ductile overload during testing.

6) The HAC mechanism varies with the increase of HJP. With HJP < 18,500, the HAC initiated in the martensitic CGHAZ with relatively high hardness and high HAC susceptibility; with 18,500 < HJP < 19,500, HAC initiated at multiple locations along the fusion boundary; and with HJP > 19,500, HAC initiated in the PGZ due to the precipitation of M_7C_3.

7) The variation of fracture morphology along the fusion boundary with the HJP corresponded to the trend curve of the time-to-failure of the samples. The HAC resistance or time-to-failure in the HJP range 18,500–19,500 is highest because the HAC initiated at fusion boundary. The fusion boundary has higher hydrogen solubility prior to HAC initiation.

8) Precipitation at the fusion boundary (PGZ) was observed for PWHT conditions 670 °C/10 h, 660 °C/50 h, and 660 °C/100 h, or in the range of HJP > 19,800. The subregion within the PGZ where precipitation occurs appears to be the preferred site for HAC initiation at high HJP values.

References

1. Dai T, Lippold JC (2018) The effect of postweld heat treatment on hydrogen-assisted cracking of F22/alloy 625 overlays. Weld J 97:75s–90s

2. Dai T, and Lippold JC (2018) Tempering behavior of the fusion boundary region of alloy 625 weld overlay on 8630 steel—accepted. Welding in the World

3. ISO, 15156-2 (2009) Petroleum and natural gas industries—materials for use in H2S-containing environments in oil and gas production—part 2: cracking-resistant carbon and low alloy steels and the use of cast irons

4. Alexandrov BT, Lippold JC, Sowards JW, Hope AT, Saltzmann DR (2013) Fusion boundary microstructure evolution associated with embrittlement of Ni–base alloy overlays applied to carbon steel. Welding World 57:39–53

5. Alexandrov B, Shi S, Rodelas JM, Lippold JC (2012) A new test for evaluation of susceptibility to hydrogen assisted cracking in dissimilar metal welds. NACE corrosion conference & expo, Houston

6. Bourgeois D (2015) Hydrogen assisted crack in dissimilar metal welds for subsea service under cathodic protection: dissertation. The Ohio State University, Columbus

7. Wang M, Akiyama E, Tsuzaki K (2007) Effect of hydrogen on the fracture behavior of high strength steel during slow strain rate test. Corros Sci 49:4081–4097

8. Symons DM (1997) Hydrogen embrittlement of Ni-Cr-Fe alloys. Metall Mater Trans A 28A:655–663

9. Symons DM (1998) The effect of carbide precipitation on the hydrogen-enhanced fracture behavior of alloy 690. Metall Mater Trans A 29A:1265–1277

10. Fenske JA (2010) Microstructure and hydrogen induced failure mechanisms in iron-nickel weldments. University of Illinois at Urbana-Champaign, Urbana

11. Dodge MF (2014) The effect of heat treatment on the embrittlement of dissimilar welded joints. Univeristy of Leicester, Leicester

12. Luppo MI, Ovejero-Garcia J (1991) The influence of microstructure on the trapping and diffusion of hydrogen in a low carbon steel. Corros Sci 32(10):1125–1136

13. Nagao A, Smith CD, Dadfarnia M, Sofronis P, Robertson IM (2012) The role of hydrogen in hydrogen embrittlement fracture of lath martensitic steel. Acta Mater 60:5182–5189

14. Lippold JC (2014) Welding metallurgy and weldability. John Wiley & Sons, Inc, Hoboken p. 215

15. Gangloff RP, Somerday BP (2012) Gaseous hydrogen embrittlement of materials in energy technologies: volume 1. Woodhead Publishing, Cambridge

16. Lynch SP (1988) Environmentally assisted cracking: overview of evidence for an adsorption-induced localised-slip process. Acta Metallugica 36(10):2639–2661

17. Lynch SP (1989) Metallographic contributions to understanding mechanisms of environmentally assisted cracking. Metallography 23(2):147–171

18. Morlet J, Johnson H, Troiano A (1958) A new concept of hydrogen embrittlement in steel. J Iron Steel Inst 189:37–44

19. Troiano A (1960) The role of hydrogen and other interstitials in the mechanical behaviour of metals. Trans ASM 52:54–80

20. Whiteman M, Troiano A (1965) Hydrogen embrittlement of austenitic stainless steel. Corrosion 21(2):53–56

21. Oriani RA, Josephic PH (1979) Hydrogen-enhanced load relaxation in a deformed medium-carbon steel. Acta Metall 27(6):997–1005

22. Oriani R (1970) The diffusion and trapping of hydrogen in steel. Acta Metall 18:147–157

23. Wriedt HA, Oriani RA (1970) Effect of tensile and compressive elastic stress on equilibrium hydrogen solubility in a solid. Acta Metall 18:753–760

24. Oriani R (1972) A mechanistic theory of hydrogen embrittlement of steels. Berichte der Bunsengesellschaft für Phys Chemie 76:848–857

25. Oriani R, Josephic P (1974) Equilibrium aspects of hydrogen-induced cracking of steels. Acta Metall 22:1065–1074

26. Beachem C (1972) A new model for hydrogen-assisted cracking (hydrogen "embrittlement"). Metall Mater Trans B 3:441–455

27. Yue X (2013) Evaluation of heat-affected zone hydrogen-induced cracking in high-strength steels—dissertation. The Ohio State University, Columbus

28. Hollomon J, Jaffe L (1945) Time-temperature relations in tempering steel. Metal Technol 12:223–249

29. Martin ML, Fenske JA, Liu GS, Sofronis P, Robertson IM (2011) On the formation and nature of quasi-cleavage fracture surfaces in hydrogen embrittled steels. Acta Mater 59:1601–1606